Time-Reversal-Breaking Weyl Fermions in Magnetic Heusler Alloys

Zhijun Wang,[1] M. G. Vergniory,[2,3] S. Kushwaha,[4] Max Hirschberger,[1] E. V. Chulkov,[2,5,7] A. Ernst,[6] N. P. Ong,[1] Robert J. Cava,[4] and B. Andrei Bernevig[1]

[1]*Department of Physics, Princeton University, Princeton, New Jersey 08544, USA*
[2]*Donostia International Physics Center, P. Manuel de Lardizabal 4, 20018 Donostia-San Sebastián, Spain*
[3]*Department of Applied Physics II, Faculty of Science and Technology, University of the Basque Country UPV/EHU, Apartado 644, 48080 Bilbao, Spain*
[4]*Department of Chemistry, Princeton University, Princeton, New Jersey 08540, USA*
[5]*Departamento de Física de Materiales, Universidad del País Vasco/Euskal Herriko Unibertsitatea UPV/EHU, 20080 Donostia-San Sebastián, Spain*
[6]*Max-Planck-Institut für Mikrostrukturphysik, Weinberg 2, D-06120 Halle, Germany*
[7]*Saint Petersburg State University, 198504 Saint Petersburg, Russia*

(Received 5 July 2016; published 30 November 2016)

Weyl fermions have recently been observed in several time-reversal-invariant semimetals and photonics materials with broken inversion symmetry. These systems are expected to have exotic transport properties such as the chiral anomaly. However, most discovered Weyl materials possess a substantial number of Weyl nodes close to the Fermi level that give rise to complicated transport properties. Here we predict, for the first time, a new family of Weyl systems defined by broken time-reversal symmetry, namely, Co-based magnetic Heusler materials XCo_2Z ($X =$ IVB or VB; $Z =$ IVA or IIIA). To search for Weyl fermions in the centrosymmetric magnetic systems, we recall an easy and practical inversion invariant, which has been calculated to be -1, guaranteeing the existence of an odd number of pairs of Weyl fermions. These materials exhibit, when alloyed, only two Weyl nodes at the Fermi level—the minimum number possible in a condensed matter system. The Weyl nodes are protected by the rotational symmetry along the magnetic axis and separated by a large distance (of order 2π) in the Brillouin zone. The corresponding Fermi arcs have been calculated as well. This discovery provides a realistic and promising platform for manipulating and studying the magnetic Weyl physics in experiments.

DOI: 10.1103/PhysRevLett.117.236401

Weyl fermions are theorized to exist in the standard model above the symmetry-breaking scale—at low-energy scales, they invariably acquire mass. As such, the search for Weyl fermions has shifted to condensed matter systems, where they appear as unremovable crossings in electronic Bloch bands, close to the Fermi level, in three spatial dimensions. They recently became a reality with the experimental discovery [1,2] of the theoretically predicted [3,4] Weyl semimetals (WSM) in the TaAs family of compounds. Topological Weyl metals are responsible for an array of exotic spectroscopic and transport phenomena such as the surface-disconnected Fermi arcs, chiral anomaly, and anomalous Hall effects [5–12].

Transport in Weyl materials reveals the fundamental nature of the Berry phase in magneto transport. The chiral anomaly is reflected in the negative longitudinal magneto-resistance (NMR), which on its own stems from the Weyl fermions. A minimum number (2) of Weyl fermions could make it easier to observe the NMR than for cases with a large number of Weyl fermions. Due to the fermion doubling problem, Weyl nodes appear in multiples of 2. With time-reversal invariance, this number increases to multiples of 4. The TaAs family of compounds exhibits 24 Weyl nodes, due to several other mirror symmetries. This large number of Weyl nodes gives rise to complicated spectroscopic and transport properties. By comparison, the hypothetical hydrogen atom of Weyl semimetals is a material with only 2 Weyl nodes at the Fermi level (E_F), preferably cleanly separated in momentum space and in energy from other bands.

In previous work [13], $HgCr_2Se_4$ has been predicted to be a Chern (*not* Weyl) semimetal with two crossing points, each of which possesses chirality of 2. The existence of only two Weyl nodes is also expected in the topological- or normal-insulator heterostructures with magnetic doping [14,15]. Unfortunately, none of these systems has been verified so far. In this Letter, we predict, for the first time, a series of magnetic Heusler compounds that can exhibit, when alloyed, two Weyl points (WPs) close to Fermi energy and largely separated in momentum space. Magnetic Heusler compounds have several advantages over the other compounds where Weyl fermions have been proposed and detected. First, they are ferromagnetic half-metallic compounds with Curie temperatures up to room temperature [16], meaning they can be of great use for spin manipulation and spintronics applications. Second, they exhibit Weyl fermions, with the large associated Berry phase of their Fermi surfaces. As such, the anomalous Hall effect and the

spin Hall effect in these materials are theoretically expected to be large, which has already been confirmed in initial experimental studies [17–19]. Third, the magnetism in these materials is "soft," meaning that an applied magnetic field can easily change the magnetic moment direction: A similar phenomenon has been observed in GdPtBi [20,21]. Since, as pointed out in the Refs. [22,43], the structure and position of Weyl fermions depends on the magnetic field, the magnetic Heusler alloys provide us with a realistic and promising platform for manipulating and studying the magnetic Weyl physics in experiments.

Based on the first-principle calculations with the magnetism oriented in the [110] direction, we found that two Weyl nodes, related by symmetry, appear on the same axis. Their energy relative to the Fermi level can be tuned by alloying, and we provide an estimation of the appropriate concentration of the dopant necessary to tune the Weyl nodes to the Fermi level. We carry out a symmetry analysis and solidify our *ab initio* claims of the existence of Weyl nodes by showing that they are formed by bands of opposite C_2 eigenvalues. Furthermore, we link the existence of Weyl nodes to the existence of an inversion invariant discovered earlier [44] in the theory of inversion symmetric topological insulators. We then obtain the structure of the Fermi arcs on the 001 surface. We expand upon the results in Ref. [22], where we also analyze the possible topological scenarios under different potential magnetization directions, and present magnetization data on one of the synthesized materials from our proposals.

Our proposed candidates for Weyl metals are the Co-based Heusler compounds: XCo_2Z (X = IVB or VB; Z = IVA or IIIA), with $N_v = 26$, denoting the number of valence electrons (s, d electrons for the transition metals and s, p electrons for the main group element). This family of Co-based Heusler compounds follows the Slater-Pauling rule, which predicts a total spin magnetic moment $m = N_v - 24$ (the number of atoms × 6) [45–47]. In this Letter, we focus on a representative candidate—$ZrCo_2Sn$, which we have synthesized experimentally [16]. We present the results for the rest of the compounds in Ref. [22]. We show that the interesting Weyl nodes of all the 26-electron compounds are about 0.6 eV above the Fermi energy. However, there is another Co-based Heusler family with 27-electron compounds that are also candidates for Weyl metals and have been synthesized experimentally [16], such as $NbCo_2Sn$ and VCo_2Sn, making it possible to move the Weyl nodes close to or at the Fermi level by alloying. The Co-based Heusler compounds, with their great diversity, give us the opportunity to tune our compounds (e.g., the number of valence electrons, spin-orbit coupling strength, etc.) across different compositions in order to get the desired properties.

We perform *ab initio* calculations based on the density functional theory (DFT) [48,49] and the generalized gradient approximation (GGA) for the exchange-correlation potential [50] (more details in Ref. [22]). The

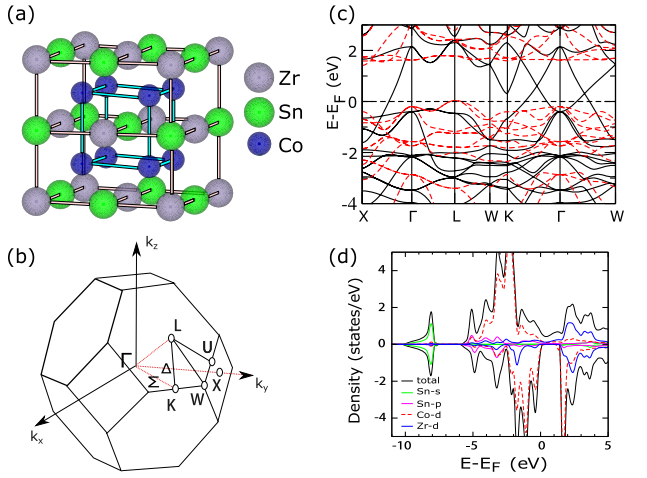

FIG. 1. (a) Rocksalt crystal structure of $ZrCo_2Sn$ with $Fm\bar{3}m$ space group. Co, Zr, and Sn atoms are shown in blue, gray, and green, respectively. (b) Brillouin zone (BZ) of the rocksalt structure. It has three independent time-reversal-invariant points, $\Gamma(0,0,0)$, $L[(\pi/a),(\pi/a),(\pi/a)]$, and $X[(2\pi/a),0,0]$. (c) Bulk band structure of $ZrCo_2Sn$ along high-symmetry lines without spin-orbit coupling (SOC). The majority and minority spin bands are indicated by solid black and dashed red lines, respectively. (d) Total and partial density of states without SOC. The positive (negative) lines represent the majority (minority) spin channel.

spin-polarized band structure and density of states (DOS) of $ZrCo_2Sn$ are calculated within GGA + U without SOC, shown in Figs. 1(c) and 1(d), respectively. The value of U was chosen to be 3 eV, which provides a Curie temperature close to the experimental value [51] and reproduces the measured magnetic moment (see Fig. 5 of Ref. [22]). The Curie temperature was computed by means of random-phase approximation by Tyablikov [52]. We have tested U with different functionals, such as LDA [53], PBE [50], and PBEsol [54], and we get the same result (detailed calculation of U as a function of T_C and the magnetic coupling constants can be found in Ref. [22]). In the following, we will use the PBE pseudopotential.

In Fig. 1(c), we see a band gap in the minority states around E_F, which has been double-checked with the modified Becke-Johnson exchange potential [55]. This suggests a good half-metallic property, which is consistent with the experimental investigation of the spin-resolved unoccupied density of states of the partner compound $TiCo_2Sn$ [56]. The calculated partial DOS, shown in Fig. 1(d), suggests the states of $ZrCo_2Sn$ around E_F are mostly of d character, namely, Co-d and Zr-d states. After including SOC, the calculated band structure in Fig. 2(c) shows the SOC has little influence on the electronic structure and the half-metallic ferromagnetism because the SOC strengths of both Co and Zr are small. We performed *ab initio* calculations to determine the energetically most favorable magnetization direction—the [110] easy axis. However, this magnetic configuration is energetically very close to the [100]. We assume the magnetism

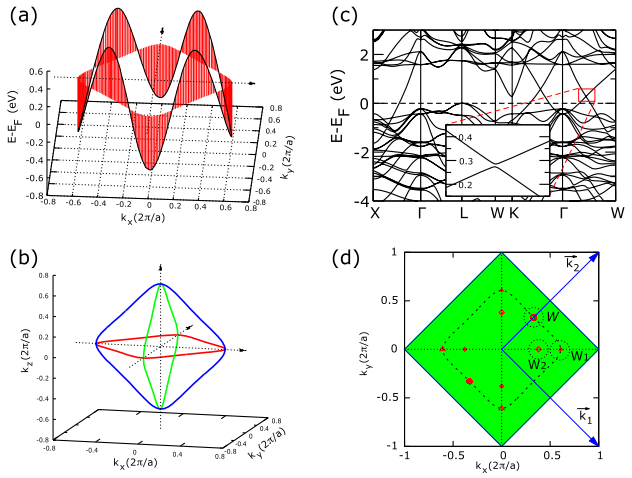

FIG. 2. (a) The nodal line in the xy plane has a big dispersion. (b) Three nodal lines in three planes in three-dimensional (3D) k space. (c) The SOC band structure of $ZrCo_2Sn$ with the [110] magnetism, opening a small gap in the ΓW direction in the inset. (d) Weyl points emerging with SOC. The independent W, W_1, and W_2 points are clearly indicated in the figure (top view)—the remaining ones can be obtained by symmetry. W and W_1 are in the xy plane, while W_2 is out of the plane. The Chern numbers can be calculated with the Wilson-loop method applied on a sphere (illustrated as dashed circles) enclosing a Weyl point. The filled (unfilled) symbols indicate Chern number $+1$ (-1). Furthermore, the 001-surface lattice vectors are also given as $\vec{k}_1[(2\pi/a), -(2\pi/a)]$ and $\vec{k}_2[(2\pi/a), (2\pi/a)]$, and the corresponding surface BZ is shown in green.

is along the [110] axis in the main text. The analysis of the [100] magnetism is presented in Ref. [22], which also shows topological properties such as Weyl points and nodal lines in the band structure.

In the spin-polarized calculation, neglecting SOC, the spin and the orbitals are independent and regarded as different subspaces. In that sense, the spatial crystal symmetries of O_h^5 have no effect on the spin degree of freedom, and the two spin channels are decoupled. Once SOC is considered, the two spin channels couple together and symmetries can decrease depending on the direction of the spontaneous magnetization. For instance, the mirror reflection M_z is a symmetry without SOC included. With SOC it is broken as the magnetization is along [110]. However, the product between time-reversal and reflection symmetries (TM_z) is still a magnetic symmetry, even though SOC is included. The corresponding magnetic space group of [110] spin polarization contains only eight elements formed by three generators: inversion $\mathcal{I}$, twofold rotation $C2_{110}$ around the 110 axis, and the product ($TC2_z$) of time reversal and rotation $C2_z$, which allows for the existence of WPs in the xy plane [57].

We first elucidate the band topology in the absence of SOC. From the spin-polarized band structure in Fig. 1(c), we can observe that two band crossings occur along ΓX, ΓW, and Γ K in the majority spin. Actually, these crossings are in the xy plane, which respects the mirror symmetry M_z. Bands within this plane can be classified by mirror eigenvalues ± 1. Further symmetry analysis shows that the two crossing bands belong to opposite mirror eigenvalues, giving rise to a nodal line in the xy plane [3,58]. The energy of the nodal line disperses dramatically in the xy plane, as shown in Fig. 2(a). The minimum of this dispersion is in the ΓX (or [100]) direction, and the maximum is in the Γ K (or [110]) direction. In addition to the nodal line in the xy plane, two similar nodal lines are also found in the xz plane and yz plane related by a $C4$ rotation around the x, y coordinate axis. As a result, the three nodal lines in different planes intersect at six different points as depicted in Fig. 2(b).

After introducing SOC, with a magnetization along the [110] direction, the mirror symmetries M_z, M_x, and M_y are all broken. In the absence of other symmetries, these nodal lines in the mirror planes would become fully gapped. However, along the magnetization [110] direction, a pair of Weyl points survive, protected by the $C2_{110}$ rotation. Namely, the crossing bands belong to different $C2_{110}$ eigenvalues $\pm i$ on the high-symmetry line. The coordinates of these WPs (W), related by inversion $\mathcal{I}$, are given in Table I. Their location and Chern numbers are illustrated in Fig. 2(d). An inversion eigenvalue argument shows us that we must have $4k + 2$, $k \in \mathcal{Z}$, number of Weyl points in this system (see Ref. [22]): The product of the inversion eigenvalues of the occupied bands at the inversion symmetric points is -1, signaling the presence of an odd number of pairs of Weyl fermions [44].

In addition, deriving from the nodal line in the xy plane, four other WPs are found slightly away from the coordinate axis in the plane. The presence of WPs in a high-symmetry plane is allowed by the antiunitary symmetry $TC2_z$ [57]. The quadruplet WPs (W_1) are related to each other by $\mathcal{I}$ and $C2_{110}$. Their precise positions and topological charges are presented in Table I. After carefully checking the other two nodal lines, we see that a third kind of Weyl point (W_2), different from the previous two kinds, does not prefer any special direction but distributes near the xz and yz plane. As

TABLE I. WPs of $ZrCo_2Sn$. The Weyl points' positions (in reduced coordinates k_x, k_y, k_z), Chern numbers, and the energy relative to the E_F of the unalloyed compound. The WPs in $ZrCo_2Sn$ are formed by two bands, which in the absence of SOC, would form nodal lines. W and W_1 are stable in the xy plane, while W_2 is stable out of the plane. The coordinates of the other Weyl points are related to the ones listed by the symmetries, $\mathcal{I}$, $C2_{110}$, and $\mathcal{T}C2_z$.

Weyl points	Coordinates $[k_x(2\pi/a), k_y(2\pi/a), k_z(2\pi/a)]$	Chern number	$E - E_F$ (eV)
W	(0.334,0.334,0)	-1	$+0.6$
W_1	$(0.58, -0.0005, 0)$	$+1$	-0.6
W_2	$(0.40, 0.001, \pm 0.28)$	-1	$+0.3$

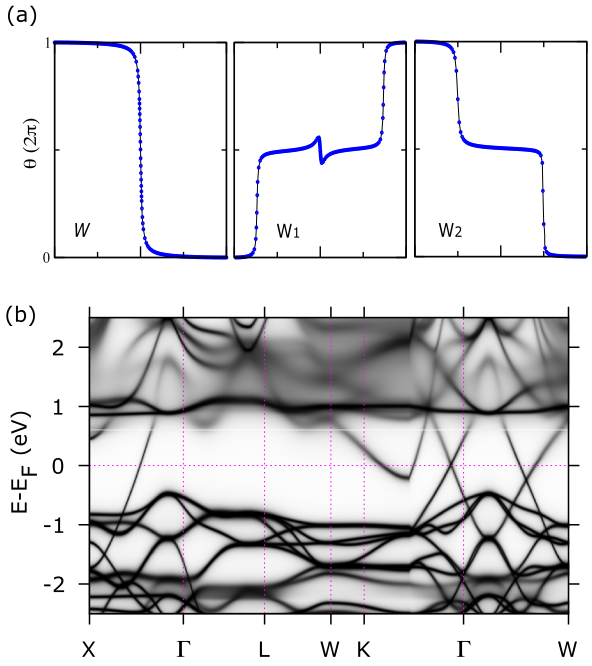

FIG. 3. (a) The flow chart of the average position of Wannier centers obtained by the Wilson-loop method applied on a sphere that encloses a node [57]. The average Wannier center shifts downwards, corresponding to Chern number -1 for W and W_2, while it shifts upwards, suggesting the Chern number of W_1 is $+1$. (b) Calculated Bloch spectral function of $Zr_{0.725}Nb_{0.275}Co_2Sn$ along high-symmetry lines.

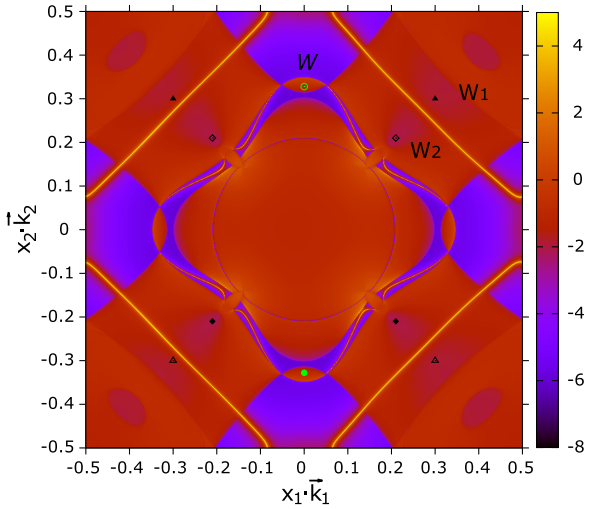

FIG. 4. Bloch spectral function of the (001) surface at 0.5 eV above the Fermi level for $ZrCo_2Sn$. In the (001)-surface Brillouin zone, the surface $\mathbf{k}$ points are represented by $x_1\vec{k}_1 + x_2\vec{k}_2$. The surface lattice vectors ($\vec{k}_1$ and $\vec{k}_2$) are illustrated, and the corresponding surface BZ is shown in green in Fig. 2(d) (notice the $\pi/2$ rotation of the surface BZ). Only the bulk projections of W (yellow) are separated from the Fermi surface projections. The bulk projections of W_1 and W_2 (black) sit inside the projection of the bulk Fermi surfaces. The Fermi arcs connecting to the bulk projections of W are shown. The large, square surface state is of a trivial nature. The color code represents $\log(\rho)$.

these WPs are generic points without any little-group symmetry, the octuplet WPs W_2 are related by all three generators of the magnetic group. As a result, the position of the W_2 changes considerably from $TiCo_2Sn$, to $ZrCo_2Sn$, to $HfCo_2Sn$, following the nodal lines without SOC. In principle, these kinds of WPs are not stable (in contrast, the W WPs are stabilized by the $C2_{110}$ symmetry on the [110] axis), as they can be moved close in the z axis and thereby annihilate with each other. The average charge centers obtained by the Wilson-loop method on the spheres (W, W_1, and W_2) are presented in Fig. 3(a). All the Chern numbers of the three WPs are shown in Table I, and their positions are shown in Fig. 2(d). As the energy level of W_1 is very low and W_2 could be removed by tuning SOC, we focus on the doublet WPs W.

We now focus on the two W WPs [located at 0.6 eV over the Fermi level in the $K-\Gamma$ (or [110]) direction]. Our goal now is to tune the energy of the WP to the Fermi level. For this purpose, we consider other compounds with the same stoichiometry, more electrons, and similar lattice parameter. As we mentioned before, $NbCo_2Sn$, which has the same crystal structure [16], contains one more electron per unit cell than $ZrCo_2Sn$. Therefore, one can expect that alloying $ZrCo_2Sn$ with Nb in the Zr site would shift down the WP energy while keeping the main band topology unchanged. Using a first-principles Green's function method, we dope $ZrCo_2Sn$ with Nb. Disorder effects were taken into account within a coherent potential approximation (CPA) [59]. Varying Nb content, we search for a concentration that brings the W WPs to the Fermi level. Figure 3(b) shows the calculated spectral function for $Zr_{1-x}Nb_xCo_2Sn$ (with $x = 0.275$). By inversion ($\mathcal{I}$) symmetry, there exists another Weyl point separated in k space by about 2π with the same energy. In the same line, the experimental existence of VCo_2Sn [16] also motivates us to dope the partner compound $Ti_{1-x}V_xCo_2Sn$ as well, and our calculations suggest $x = 0.1$.

Given that the Weyl nodes W, W_1, and W_2 all resulted from the connected nodal lines in the absence of SOC, a large residual Fermi surface has a projection on any surface of the material. Hence, the Fermi arcs emanating from the W Weyl points are interrupted by the residual projection of bulk Fermi surfaces on the surface of the material. However, the Fermi arc signatures of W WPs are still clear, as can be seen in Fig. 4 where we plot the surface spectral function for the (001) surface of $ZrCo_2Sn$. Since the bulk Fermi surface projections where W_1 and W_2 are located overlap, the Fermi arc connections are not guaranteed at certain energies. Furthermore, a trivial square surface state is found as well, due to the hanging bonding at the surface.

In conclusion, we have predicted theoretically that a new family of Co-based magnetic Heusler alloys realize Weyl systems with several Weyl nodes whose position in energy

can be tuned by alloying. We have performed *ab initio* calculations of a representative ferromagnetic compound $ZrCo_2Sn$. For the [110] magnetization we find two Weyl points related by $\mathcal{I}$ symmetry situated on the same axis. By means of a first-principles Green's function method, we doped the $ZrCo_2Sn$ with Nb and showed that these two Weyl nodes can be shifted to the Fermi level. Finally, we obtained the Fermi arc structure of this class of materials. This discovery shows a way to realize the hydrogen atom of Weyl materials and provides a promising platform for studying exotic properties of magnetic Weyl fermions in experiments.

We thank Zhida Song for providing the overlap calculating code. Z. W. and B. A. B. were supported by the Department of Energy Grant No. DE-SC0016239, the National Science Foundation EAGER Grant No. NOA-AWD1004957, Simons Investigator Grants No. ONR-N00014-14-1-0330, No. ARO MURI W911NF-12-1-0461, and No. NSF-MRSEC DMR-1420541, the Packard Foundation, the Schmidt Fund for Innovative Research, and the National Natural Science Foundation of China (No. 11504117). M. G. V. and E. V. C. acknowledge partial support from the Basque Country Government, Departamento de Educación, Universidades e Investigación (Grant No. IT-756-13), the Spanish Ministerio de Economía e Innovación (Grants No. FIS2010-19609-C02-01 and No. FIS2013-48286-C2-1-P), FEDER funding, and the St. Petersburg State University (Project No. 15.61.202.2015). A. E. acknowledges the Joint Initiative for Research and Innovation within the Fraunhofer and Max Planck cooperation program and the DFG Priority Program 1666 "Topological Insulators." R. J. C. and N. P. O. were supported by a MURI grant for topological insulators (No. ARO W911NF-12-1-0461).

Z. W. and M. G. V. contributed equally to this work.

[1] B. Q. Lv *et al.*, Phys. Rev. X **5**, 031013 (2015).
[2] S.-Y. Xu *et al.*, Science **349**, 613 (2015).
[3] H. Weng, C. Fang, Z. Fang, B. A. Bernevig, and X. Dai, Phys. Rev. X **5**, 011029 (2015).
[4] S.-M. Huang *et al.*, Nat. Commun. **6**, 7373 (2015).
[5] H. Nielsen and M. Ninomiya, Phys. Lett. B **130B**, 389 (1983).
[6] X. Wan, A. M. Turner, A. Vishwanath, and S. Y. Savrasov, Phys. Rev. B **83**, 205101 (2011).
[7] J. Xiong, S. K. Kushwaha, T. Liang, J. W. Krizan, M. Hirschberger, W. Wang, R. J. Cava, and N. P. Ong, Science **350**, 413 (2015).
[8] X. Huang *et al.*, Phys. Rev. X **5**, 031023 (2015).
[9] J. Liu and D. Vanderbilt, Phys. Rev. B **90**, 155316 (2014).
[10] M. Hirayama, R. Okugawa, S. Ishibashi, S. Murakami, and T. Miyake, Phys. Rev. Lett. **114**, 206401 (2015).
[11] T. C. V. Bzdušek, A. Rüegg, and M. Sigrist, Phys. Rev. B **91**, 165105 (2015).
[12] A. A. Burkov, Phys. Rev. Lett. **113**, 187202 (2014).
[13] G. Xu, H. Weng, Z. Wang, X. Dai, and Z. Fang, Phys. Rev. Lett. **107**, 186806 (2011).
[14] A. A. Burkov and L. Balents, Phys. Rev. Lett. **107**, 127205 (2011).
[15] D. Bulmash, C.-X. Liu, and X.-L. Qi, Phys. Rev. B **89**, 081106 (2014).
[16] A. Carbonari, R. Saxena, W. Pendl, J. M. Filho, R. Attili, M. Olzon-Dionysio, and S. de Souza, J. Magn. Magn. Mater. **163**, 313 (1996).
[17] S. Wurmehl, G. H. Fecher, H. C. Kandpal, V. Ksenofontov, C. Felser, H.-J. Lin, and J. Morais, Phys. Rev. B **72**, 184434 (2005).
[18] T. Graf, J. Winterlik, L. Muchler, G. H. Fecher, C. Felser, and S. S. P. Parkin, Handb. Magn. Mat. **21**, 1 (2013).
[19] W. Zhang, Z. Qian, Y. Sui, Y. Liu, W. Su, M. Zhang, Z. Liu, G. Liu, and G. Wu, J. Magn. Magn. Mater. **299**, 255 (2006).
[20] C. Shekhar *et al.*, arXiv:1604.01641.
[21] M. Hirschberger, S. Kushwaha, Z. Wang, Q. Gibson, S. Liang, C. A. Belvin, B. A. Bernevig, R. J. Cava and N. P. Ong, Nat. Mater. **15**, 1161 (2016).
[22] See Supplemental Material at http://link.aps.org/supplemental/10.1103/PhysRevLett.117.236401, which includes Refs. [23–42], for the details on the band structures of other candidates, detailed calculation methods, experimental measurements, inversion symmetry characterization, and symmetry analysis. The results of 100-magnetism are presented as well.
[23] E. Goerlich, R. Kmiec, K. Latka, T. Matlak, K. Ruebenbauer, A. Szytula, and K. Tomala, Phys. Status Solidi A **30**, 765 (1975).
[24] E. Goerlich, K. Latka, D. Szytula, A. Wagner, R. Kmiec, and K. Ruebenbauer, Solid State Commun. **25**, 661 (1978).
[25] P. Webster and K. Ziebeck, J. Phys. Chem. Solids **34**, 1647 (1973).
[26] K. Buschow, P. Van Engen, and R. Jongebreur, J. Magn. Magn. Mater. **38**, 1 (1983).
[27] K. Buschow and P. Van Engen, J. Magn. Magn. Mater. **25**, 90 (1981).
[28] G. Kresse and J. Furthmueller, Comput. Mater. Sci. **6**, 15 (1996).
[29] G. Kresse and J. Hafner, Phys. Rev. B **48**, 13115 (1993).
[30] G. Kresse and D. Joubert, Phys. Rev. B **59**, 1758 (1999).
[31] D. Hobbs, G. Kresse, and J. Hafner, Phys. Rev. B **62**, 11556 (2000).
[32] S. L. Dudarev, G. A. Botton, S. Y. Savrasov, C. J. Humphreys, and A. P. Sutton, Phys. Rev. B **57**, 1505 (1998).
[33] P. G. van Engen, K. H. J. Buschow, and M. Erman, J. Magn. Magn. Mater. **30**, 374 (1983).
[34] J. Korringa, Physica (Amsterdam) **13**, 392 (1947).
[35] W. Kohn and N. Rostoker, Phys. Rev. **94**, 1111 (1954).
[36] M. Lueders, A. Ernst, W. M. Temmerman, Z. Szotek, and P. J. Durham, J. Phys. Condens. Matter **13**, 8587 (2001).
[37] A. I. Liechtenstein, M. I. Katsnelson, and V. A. Gubanov, J. Phys. F **14**, L125 (1984).
[38] R. V. Skolozdra, Y. V. Stadnyk, Y. K. Gorelenko, and E. E. Treletskaya, Sov. Phys. Solid State **32**, 1536 (1990).
[39] K. Momma and F. Izumi, J. Appl. Crystallogr. **44**, 1272 (2011).
[40] T. Williams, C. Kelley *et al.*, Gnuplot 4.4: An interactive plotting program, http://gnuplot.sourceforge.net (2010).
[41] F. Munoz and A. Romero, *Pyprocar* (2014).

[42] P. Ramachandran and G. Varoquaux, Comput. Sci. Eng. **13**, 40 (2011).
[43] S. Chadov, G. H. Fecher, and C. Felser (private communication).
[44] T. L. Hughes, E. Prodan, and B. A. Bernevig, Phys. Rev. B **83**, 245132 (2011).
[45] S. Skaftouros, K. Özdoğan, E. Şaşıoğlu, and I. Galanakis, Phys. Rev. B **87**, 024420 (2013).
[46] I. Galanakis, P. H. Dederichs, and N. Papanikolaou, Phys. Rev. B **66**, 174429 (2002).
[47] G. H. Fecher, H. C. Kandpal, S. Wurmehl, C. Felser, and G. Schoenhense, J. Appl. Phys. **99**, 08J106 (2006).
[48] P. Hohenberg and W. Kohn, Phys. Rev. **136**, B864 (1964).
[49] W. Kohn and L. J. Sham, Phys. Rev. **140**, A1133 (1965).
[50] J. P. Perdew, K. Burke, and M. Ernzerhof, Phys. Rev. Lett. **77**, 3865 (1996).
[51] E. Uchida, N. Fukuoka, H. Kondoh, T. Takeda, Y. Nakazumi, and T. Nagamiya, J. Phys. Soc. Jpn. **19**, 2088 (1964).
[52] S. V. Tyablikov, *Methods in the Quantum Theory of Magnetism* (Springer Science, Plenum, New York, 1967).
[53] J. P. Perdew and A. Zunger, Phys. Rev. B **23**, 5048 (1981).
[54] J. P. Perdew, K. Burke, and M. Ernzerhof, Phys. Rev. Lett. **80**, 891 (1998).
[55] F. Tran and P. Blaha, Phys. Rev. Lett. **102**, 226401 (2009).
[56] P. Klaer, M. Kallmayer, C. G. F. Blum, T. Graf, J. Barth, B. Balke, G. H. Fecher, C. Felser, and H. J. Elmers, Phys. Rev. B **80**, 144405 (2009).
[57] A. A. Soluyanov, D. Gresch, Z. Wang, Q. Wu, M. Troyer, X. Dai, and B. A. Bernevig, Nature (London) **527**, 495 (2015).
[58] G. Bian *et al.*, Nat. Commun. **7**, 10556 (2016).
[59] B. L. Gyorffy, Phys. Rev. B **5**, 2382 (1972).